

CO₂-broadening coefficients in the ν_4 fundamental band of methane at room temperature and application to CO₂-rich planetary atmospheres



Laurent Fissiaux^{a,1}, Quentin Delière^{a,b}, Ghislain Blanquet^a, Séverine Robert^b, Ann Carine Vandaele^b, Muriel Lepère^{a,*}

^a Laboratoire Lasers et Spectroscopies (LLS), Research centre in Physics of Matter and Radiation (PMR), University of Namur, 61, rue de Bruxelles, B-5000 Namur, Belgium

^b Planetary Aeronomy, Belgian Institute for Space Aeronomy (IASB-BIRA), 3, Avenue Circulaire, B-1180 Bruxelles, Belgium

ARTICLE INFO

Article history:

Received 7 November 2013

In revised form 26 December 2013

Available online 14 January 2014

Keywords:

Collisional broadenings

CH₄

Carbon dioxide

Planetary atmospheres

ExoMarsTGO

NOMAD

Diode-laser

ABSTRACT

Using a tunable diode-laser spectrometer, we have measured the CO₂-broadening coefficients of 28 absorption lines in the ν_4 band of CH₄. Each line was recorded at room temperature (296 K) and at 4 different pressures, ranging from 8 to 50 mbar. The experimental determination of the CO₂-broadening coefficients was performed by fitting a theoretical profile to the experimental profile of each line recorded at each pressure. Voigt, Rautian–Sobel'man and Galatry models were therefore used. The impact of these determinations on atmospheric investigations on CO₂-rich planetary atmospheres are addressed.

© 2014 Elsevier Inc. All rights reserved.

1. Introduction

The study of planetary atmospheres is a hot topic and spectroscopy is a powerful discipline to gain insight into it. Instruments on board various spacecrafts sound these atmospheres in different wavelength ranges, from the UV to the IR, under various geometry, solar or stellar occultation, limb and nadir to obtain detailed composition and even dynamics. To retrieve physical properties, atmospheric spectra must be analyzed with accurate spectroscopic line parameters. In particular, broadening coefficients associated to their adequate line profile are of high importance [1].

The European Venus Express mission [2], with the SOIR instrument [3] on board, has been in orbit round Venus since 2006 and still provides a lot of new information on the planet and in particular on its atmosphere. A new absorption band of CO₂ was discovered in SOIR spectra [4] and also seen in Martian data [5], in the same spectral region as the ν_3 band of methane. This contributed to a better characterization of the spectra in these wavelengths and in consequence led to a better knowledge in the search for methane on Mars as evidenced in recent observations of methane in the Martian atmosphere [6,7]. This discovery, which is still

controversial and poorly understood [8], was one of the starting points for the definition of the new mission to Mars, the “ExoMars Trace Gas Orbiter” (EMTGO) mission [9] to be launched in 2016. The origin of methane on Mars is still uncertain: it could be produced from internal processes like volcanoes or serpentinization, from biological processes or from exogeneous sources like cometary impacts [10]. The 2 infra-red channels of the NOMAD instrument [11], which will be part of the payload of the EMTGO mission, are designed to measure atmospheric transmission in the near-IR (2.2–4.3 μm) at high resolution (0.12–0.30 cm^{-1}) through solar occultation and nadir observations [12]. They therefore allow the derivation of unique remote sensing information about the vertical structure and composition of the Martian atmosphere with very good spatial resolution.

The previous studies of methane collisional broadening coefficients in the ν_4 fundamental band were devoted to the CH₄–CH₄, CH₄–N₂, CH₄–O₂ and CH₄–Ar mixtures [13–16]. These works are especially useful for the Earth atmosphere, but less for the Martian atmosphere which is mainly composed of CO₂ (96%). The determination of the densities of methane relies on the knowledge of accurate and adapted spectroscopic data, requiring, in particular for Mars, CO₂ broadening coefficients of high quality.

Using a tunable diode-laser spectrometer, we have studied 28 lines of ν_4 band of CH₄ ranging between P(11) and R(12) and located between 1241.861 and 1368.948 cm^{-1} . This experimental

* Corresponding author. Fax: +32 81 72 45 85.

E-mail address: muriel.lepere@unamur.be (M. Lepère).

¹ Postdoctoral Researcher with the F.R.S.-FNRS (Belgium).

method presents two essential advantages: a high effective resolution ($\pm 5.10^{-4} \text{ cm}^{-1}$) and the possibility to use the “line-by-line” method. We can adapt the experimental parameters (pressure and path length) to obtain optimal absorption and to avoid systematic errors. To deduce the broadening of the studied line, we fitted a Voigt, a Rautian and a Galatry profile to the experimental one. Simulations of the ν_3 band have been performed using a code called ASIMUT-ALVL, software developed at IASB-BIRA [17] and taking into account the new set of broadening coefficients.

2. Experimental details

The spectra were recorded with an improved tunable diode-laser spectrometer (TDL) interfaced to a PC computer and described in details in [18,19]. A homemade microprocessor signal average working at a sweep frequency of 13.5 Hz was used for data acquisition. In order to increase the signal-to-noise ratio, each spectrum was averaged over 100 scans. For the relative calibration, a confocal etalon with a free spectral range of 0.008323 cm^{-1} was introduced in the laser beam. The $^{12}\text{CO}_2$ sample was provided by *Air products* with a stated purity of 99.6% and the CH_4 sample was provided by *Air Liquid* with a stated purity of 99.95%. The optical path length (4.17 m) was obtained with a 1 m White-type cell. Depending on the line under study, pressures of methane and carbon dioxide were chosen between 0.0217 and 0.1851 mbar and between 8 and 50 mbar respectively. The pressure was measured by two MKS baratron gauges with a full scale reading of 1.3 and 130 mbar. All the spectra were recorded at room temperature ($296 \pm 1 \text{ K}$).

For each studied line, we recorded eight consecutive spectra:

1. The empty cell giving the laser emission profile (100% of transmission).
2. The line at a very low pressure and a weak absorption which provides an observed Doppler profile, convolution of the true Doppler profile with the apparatus function.
- 3–6. The broadened CH_4 line at four different pressures of carbon dioxide.
7. The étalon fringe with the absorption cell evacuated.
8. The saturated line giving the 0% transmission level.

The assignments and wavenumbers of the studied lines have been taken from HITRAN database [20]. Fig. 1 shows an example

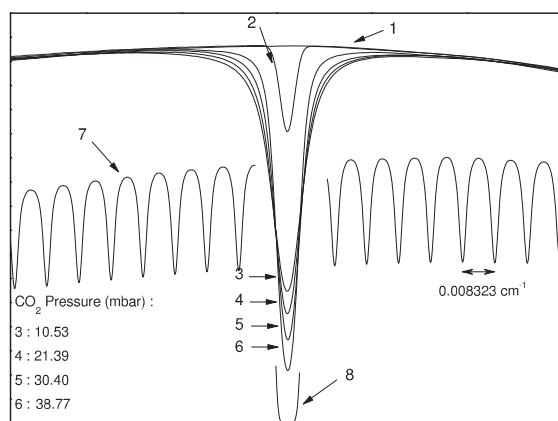


Fig. 1. Example of spectra recorded for the P(6)-E line in the ν_4 band of CH_4 at room temperature: (1) diode-laser emission profile, (2) spectrum of pure CH_4 line recorded at low pressure and absorption and used to determine the apparatus function, (3–6) spectra of the CH_4 line at different pressures of $^{12}\text{CO}_2$ (10.53, 21.39, 30.40, 38.77 mbar), (7) record of the confocal étalon fringes used for relative calibration in wavenumber, (8) 0% transmission level.

of the spectra recorded for the P(6)-E line in the ν_4 band at 1271.588 cm^{-1} . The fringe pattern has allowed to correct the slightly nonlinear tuning of the diode with a constant step of about $1 \times 10^{-4} \text{ cm}^{-1}$. The purity of the mode was checked by the smoothness of the étalon fringe pattern, the laser emission regularity and the level of a saturated line.

3. Data reduction

The experimental absorbance $\alpha(\tilde{\nu})$ can be deduced for each perturber pressure using the Beer–Lambert’s law as

$$\alpha(\tilde{\nu}) = -\ln \left(\frac{I_t(\tilde{\nu})}{I_0(\tilde{\nu})} \right) \quad (1)$$

where $I_0(\tilde{\nu})$ and $I_t(\tilde{\nu})$ are the spectral irradiance (in W m^{-1}) of a collimated beam respectively before and after absorption by the gaseous sample and $\tilde{\nu}$ is the wavenumber (in cm^{-1}).

The line parameters were obtained by fitting a theoretical line-shape to the measured absorbance. First, we used the Voigt profile [21]. This profile is simply the convolution of a Gauss function (Doppler effect) by a Lorentz function (collisional effect), assuming that both effects are independent. It can be defined as [22]:

$$\alpha_V(A, x, y) = A \frac{y}{\pi} \int_{-\infty}^{+\infty} \frac{\exp(-t^2)}{y^2 + (x-t)^2} dt = A \text{Re}[W(x, y)] \quad (2)$$

with

$$W(x, y) = \frac{i}{\pi} \int_{-\infty}^{+\infty} \frac{\exp(-t^2)}{x + iy - t} dt \quad (3)$$

and

$$A = \frac{S\sqrt{\ln 2}}{\gamma_D\sqrt{\pi}}; \quad y = \sqrt{\ln 2} \frac{\gamma_C}{\gamma_D}; \quad x = \sqrt{\ln 2} \frac{\tilde{\nu} - \tilde{\nu}_0}{\gamma_D} \quad (4)$$

where S is the line intensity (in cm^{-2}), γ_C (in cm^{-1}) is the collisional half-width, γ_D is the Doppler half-width and $\tilde{\nu}_0$ is the line center wavenumber (in cm^{-1}).

However, Doppler and collisional effects are not independent and intermolecular collisions perturb the Doppler effect. The mean translation motion of the active molecules is reduced and the free streaming motion of the molecules becomes diffuse. This is well known as the Dicke effect [23]. We also fit the experimental profiles using the Rautian and Sobel’man [24] and Galatry [25] models taking into account the Dicke effect.

The Rautian and Sobel’man model is also called hard collision model because it assumes that the velocity of the active molecule after the collision is independent of its velocity before the collision. This model is best suited when the perturber mass is larger than the mass of the active molecule. This profile may be described as [24]:

$$\alpha_R(A, x, y, z) = A \text{Re} \left[\frac{W(x, y + z)}{1 - \sqrt{\pi}zW(x, y + z)} \right] \quad (5)$$

where the parameters W , A , x and y are the same as defined in Eqs. (3) and (4) and

$$z = \sqrt{\ln 2} \frac{\beta_C}{\gamma_D} \quad (6)$$

with β_C (in cm^{-1}) representing the average effect of collisions on Doppler broadening.

The Galatry model is also called soft collision model because it assumes that the duration of each collision is short and does not modify significantly the velocity of the active molecule. This

second model is best suited when the active molecule mass is larger than the perturber one. It can be defined by [25]

$$\alpha_G(A, x, y, z) = \frac{A}{\sqrt{\pi}} \operatorname{Re} \left[\int_{-\infty}^{+\infty} \exp \left(-ixt - yt - \frac{zt - 1 + e^{-zt}}{2z^2} \right) dt \right] \quad (7)$$

with the same definition of the parameters.

In order to take into account the instrumental distortions, the effective Doppler half-width was fixed in the fitting procedure to the γ_D value given by [26]

$$\gamma_D = \sqrt{(\gamma_{DT}^2 + \gamma_{App}^2)} \quad (8)$$

where γ_{App} is the contribution due to the instrument distortion [27] and where γ_{DT} is the theoretical Doppler broadening coefficient defined as

$$\gamma_{DT} = 3.581 \times 10^{-7} \tilde{\nu}_0 \sqrt{\frac{T}{M}} \quad (9)$$

with $\tilde{\nu}_0$ (in cm^{-1}) the wavenumber of the measured transition, T (in K) the temperature, M (in a.m.u) the molecular mass.

The apparatus half-width was determined by fitting a function $\alpha(\tilde{\nu} - \tilde{\nu}_0)$ to the absorbance line recorded at very small pressure and absorption:

$$\alpha(\tilde{\nu} - \tilde{\nu}_0) = -\ln \left[\int_{-\infty}^{+\infty} f_{App}(\tilde{\nu}_i) \exp(-k_{Dop}(\tilde{\nu} - \tilde{\nu}_0 - \tilde{\nu}_i)L) d\tilde{\nu}_i \right] \quad (10)$$

with L the absorption length, $f_{App}(\tilde{\nu}_i)$ the Gaussian instrumental profile with an adjustable half-width γ_{App} and $k_{Dop}(\tilde{\nu} - \tilde{\nu}_0)$ the theoretical Gaussian Doppler profile. For this study, γ_{App} varied from 0.3 to $0.7 \times 10^{-3} \text{ cm}^{-1}$.

Fig. 2 presents an example of the theoretical profiles fitted on the observed absorbance for the P(6)-E line in the ν_4 band of CH_4 . As expected, the Rautian and the Galatry profiles incorporating the Dicke [23] effect are in better adequacy than the Voigt profile.

4. Experimental results

The collisional half-width at half-maximum determined is determined by the relation:

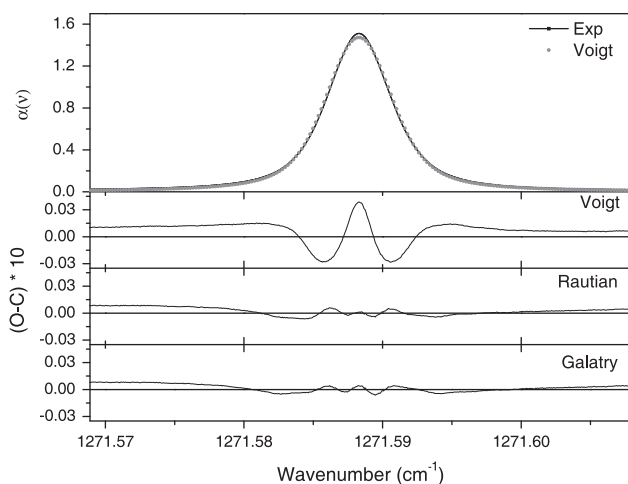


Fig. 2. The measured absorbance for the P(6)-E line in the ν_4 band of CH_4 ($p = 0.0472$ mbar) perturbed by 10.53 mbar of CO_2 (-), and the adjusted Voigt profile (\bullet). Residuals, calculated as the difference between observed and fitted values, are multiplied by 10 and represented at the bottom for the Voigt, the Rautian and the Galatry profiles.

$$\gamma_C = \gamma_0 * p_{\text{CO}_2} + \gamma_{\text{self}} * p_{\text{CH}_4} \quad (11)$$

with γ_0 the CO_2 -broadening coefficients, γ_{self} the self-broadening coefficient, p_{CO_2} the CO_2 pressure and p_{CH_4} the CH_4 pressure.

For a given line, the collisional HWHM γ_C was determined for at least four perturber pressures. Fig. 3 shows a typical plot of $\gamma_C - \gamma_{\text{self}} * p_{\text{CH}_4}$ versus the CO_2 pressure for the P(6)-E line of the ν_4 band of CH_4 . The self-broadening contribution was evaluated from the results given by Smith et al. [28] and is represented by the point passes through the origin. The slopes of the straight lines obtained from the best linear regressions give the CO_2 -broadening coefficients. These results are presented in Table 1 along with their experimental errors. These errors have been estimated to be twice the standard deviation derived from the linear regression plus 2% of γ_0 to take into account the whole experimental uncertainties. The main sources of uncertainties in the determination of the parameters arise from the baseline position, the perturbation due to the neighboring lines, the lineshape model used, the slightly nonlinear tuning of the laser. The values obtained with Rautian line shape are very close to those deduced from Galatry fits but the values deduced from Voigt fits are systematically smaller than those obtained with Rautian (or Galatry) fits. Because Rautian and Sobel'-man and Galatry models represent limit cases about mass ratio, in intermediate cases, the values determined by both models are almost very close.

Finally, Fig. 4 presents the CO_2 -broadening coefficients γ_0 versus m number ($m = -J$ for P-branch and $J + 1$ for R-branch) respectively for A, E and F symmetry. Solid symbols represent P-branch and open symbols are for R-branch. As usual, the coefficients γ_0 decrease with increasing $|m|$ values.

5. Application to planetary atmospheres

Remote sensing techniques are more and more sensitive. NO-MAD's resolution (0.10 cm^{-1} in solar occultation mode and 0.40 cm^{-1} in nadir mode) for instance will be of one order magnitude higher than that of PFS (1.3 cm^{-1}) onboard Mars Express. This higher resolution should enable us to better characterize the composition of the martian atmosphere and dispel the doubt about the methane detection, if any. As the search for methane in the martian atmosphere is a key issue in the EMTGO 2016 mission, we

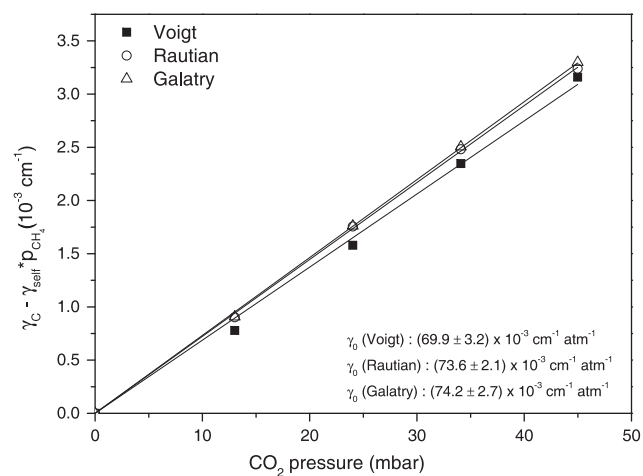


Fig. 3. CO_2 -collisional halfwidths $\gamma_C - \gamma_{\text{self}} * p_{\text{CH}_4}$ (in 10^{-3} cm^{-1}) versus the pressure (in mbar) for the P(6)-E line of CH_4 in the ν_4 band at room temperature. The values obtained with the Voigt (\blacksquare), the Rautian (\circ) and the Galatry (\triangle) profiles are represented here. The slopes of the best-fit lines represent the CO_2 -broadening coefficients.

Table 1
CO₂-broadening coefficients in the ν_4 band of CH₄.

Line	$J' C'$	n'	$J'' C''$	n''	Wavenumber ^a (cm ⁻¹)	γ_0 (10 ⁻³ cm ⁻¹ atm ⁻¹)		
						Voigt ^b	Rautian ^b	Galatry ^b
R(12)-A ₂	13 A1	1	12 A2	1	1368.9483	58.9 ± 3.9	61.9 ± 2.2	61.9 ± 3.2
R(8)-A ₁	9 A2	1	8 A1	1	1353.1590	60.3 ± 3.2	64.8 ± 1.7	65.1 ± 1.9
R(7)-A ₂	8 A1	1	7 A2	1	1347.0542	64.8 ± 3.9	68.0 ± 2.0	68.4 ± 2.4
R(7)-F ₂	8 F1	1	7 F2	2	1346.7396	72.8 ± 3.6	75.3 ± 1.7	75.5 ± 1.9
R(7)-E	8 E	1	7 E	1	1346.5755	54.3 ± 3.8	58.3 ± 1.6	58.6 ± 2.0
R(6)-A ₂	7 A1	1	6 A2	1	1342.6545	66.1 ± 4.9	70.1 ± 1.8	70.3 ± 2.2
R(5)-F ₁	6 F2	2	5 F1	1	1337.8238	72.1 ± 2.8	74.9 ± 2.3	75.0 ± 2.7
R(5)-F ₂	6 F1	1	5 F2	1	1337.5950	75.7 ± 3.1	78.6 ± 3.0	78.9 ± 3.4
R(4)-F ₂	5 F1	1	4 F2	1	1332.0853	72.8 ± 4.8	76.7 ± 1.9	76.9 ± 2.9
R(1)-F ₁	2 F2	1	1 F1	1	1316.8272	76.1 ± 3.1	80.0 ± 2.4	80.5 ± 3.0
P(1)-F ₁	0 F2	1	1 F1	1	1300.2800	76.3 ± 5.3	79.8 ± 2.8	80.0 ± 2.4
P(3)-F ₁	2 F2	2	3 F1	1	1288.9509	79.7 ± 5.7	84.0 ± 3.1	84.3 ± 2.5
P(3)-F ₂	2 F2	2	3 F2	1	1288.4570	80.5 ± 4.2	84.4 ± 2.3	84.6 ± 3.1
P(3)-A ₂	2 A1	1	3 A2	1	1287.8133	76.0 ± 4.3	79.3 ± 2.6	79.4 ± 2.4
P(4)-A ₁	3 A2	1	4 A1	1	1283.4588	75.5 ± 3.5	78.7 ± 2.2	79.0 ± 2.8
P(4)-F ₁	3 F2	2	4 F1	1	1282.9842	79.8 ± 4.4	82.0 ± 2.4	82.1 ± 2.2
P(5)-E	4 E	2	5 E	1	1275.3868	67.2 ± 5.3	69.6 ± 2.2	69.7 ± 2.0
P(5)-F ₁	4 F2	3	5 F1	2	1275.0417	75.2 ± 4.3	77.9 ± 2.2	77.9 ± 2.4
P(6)-E	5 E	3	6 E	1	1271.5894	69.9 ± 3.2	73.6 ± 2.1	74.2 ± 2.7
P(6)-A ₂	5 A1	1	6 A2	1	1270.7850	70.3 ± 4.6	73.0 ± 1.9	73.0 ± 2.5
P(7)-A ₂	6 A1	2	7 A2	1	1263.3274	66.1 ± 4.5	68.7 ± 2.4	68.8 ± 1.8
P(7)-F ₂	6 F1	4	7 F2	2	1262.2285	74.6 ± 2.9	76.9 ± 2.6	77.0 ± 3.1
P(8)-F ₁	7 F2	5	8 F1	1	1259.6616	67.4 ± 4.3	70.5 ± 2.0	70.6 ± 2.2
P(8)-E	7 E	4	8 E	1	1259.5253	64.2 ± 3.2	66.8 ± 1.9	67.0 ± 2.9
P(9)-E	8 E	4	9 E	1	1250.0011	60.2 ± 3.2	62.7 ± 1.3	62.9 ± 1.8
P(10)-E	9 E	4	10 E	2	1238.0224	46.7 ± 4.1	51.1 ± 1.8	51.2 ± 2.6
P(11)-F ₁	10 F2	8	11 F1	1	1241.9489	56.1 ± 4.3	60.7 ± 1.8	61.2 ± 2.0
P(11)-F ₂	10 F1	8	11 F2	1	1241.8632	52.3 ± 4.2	57.5 ± 1.9	58.0 ± 2.2

^a Line wavenumbers are taken from [20].

^b The experimental uncertainties are twice the standard deviation from the linear regression and a additional 2% of γ_0 .

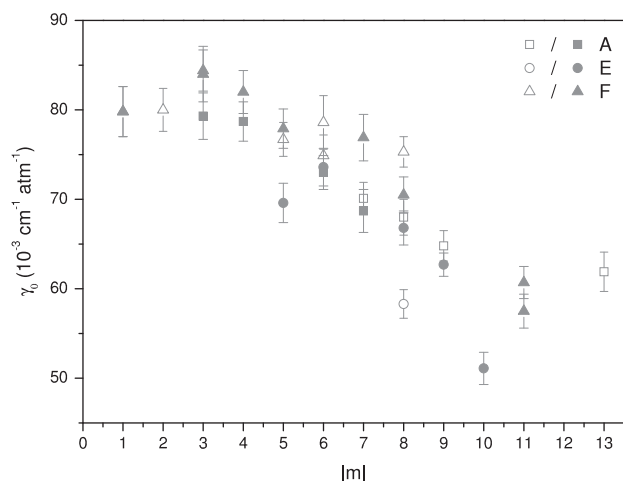


Fig. 4. CO₂-broadening coefficients γ_0 in the ν_4 band of methane at room temperature versus m ($m = -J$ for P-branch and $J + 1$ for R-branch). Solid symbols represent P-branch and open symbols are for R-branch. These coefficients are determined by Rautian fits. The error bars are two times the standard deviation given by the linear regression plus two percents of the coefficient γ_0 .

investigated the effect of a better set of line parameters onto the spectra simulated in the two viewing modes.

In the analysis performed by Formisano et al. [6] and Mumma et al. [7], atmospheric spectra were confronted to simulated ones using HITRAN 2008 line parameters to deduce methane column density. In this work, we used two kinds of line parameters: HITRAN 2008 [29] and those retrieved for the 28 lines measured in the laboratory in Namur. Taken into account the spectral range of NOMAD, i.e. 2250–4500 cm⁻¹, we applied the broadening

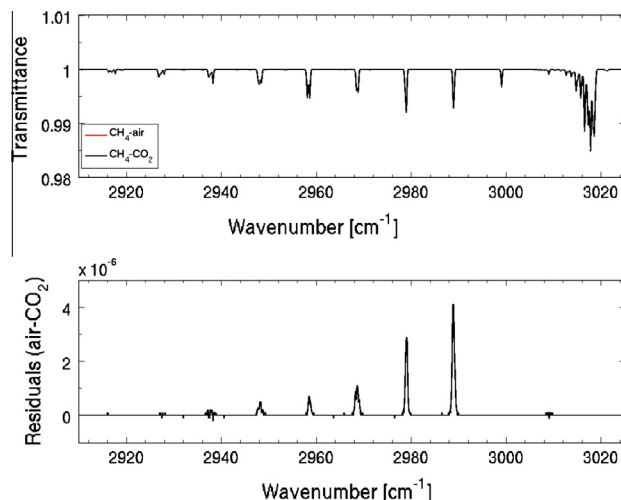


Fig. 5. ASIMUT simulations of the ν_3 band of CH₄ (30 ppb) in the Nadir mode at a spectral resolution of 0.30 cm⁻¹ using the conventional HITRAN parameters (air-broadened, red curve) and the data obtained in this work (CO₂-broadened, black curve). Zoom on the P- and Q-branch. The plots at the bottom represent the difference between the red and the black curve. (For interpretation of the references to color in this figure legend, the reader is referred to the web version of this article.)

parameters measured in the laboratory for the ν_4 band to the ν_3 band, respectively centered around 1306 cm⁻¹ and 3019 cm⁻¹. With respect to the rotational assignment, the broadening parameters were modified for 162 lines of the ν_3 band. All lines of the ν_3 band having the same rotational quanta J and C as a measured line of the ν_4 band were edited, regardless the value of α , the counting integer described in [30]. This implies to assume a vibrational non-dependence of the broadening parameters. Considering the

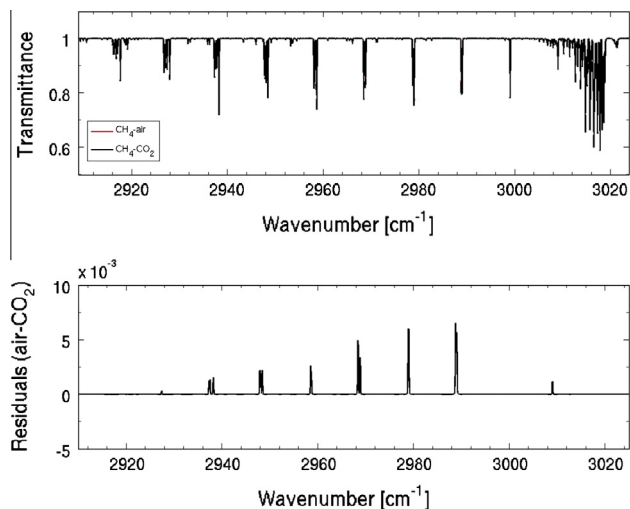


Fig. 6. ASIMUT simulations of the ν_3 band of CH_4 (30 ppb) in the solar occultation mode at a spectral resolution of 0.10 cm^{-1} using the conventional HITRAN parameters (air-broadened, red curve) and the data obtained in this work (CO_2 -broadened, black curve). Zoom on the P- and Q-branch. The plots at the bottom represent the difference between the red and the black curve. (For interpretation of the references to color in this figure legend, the reader is referred to the web version of this article.)

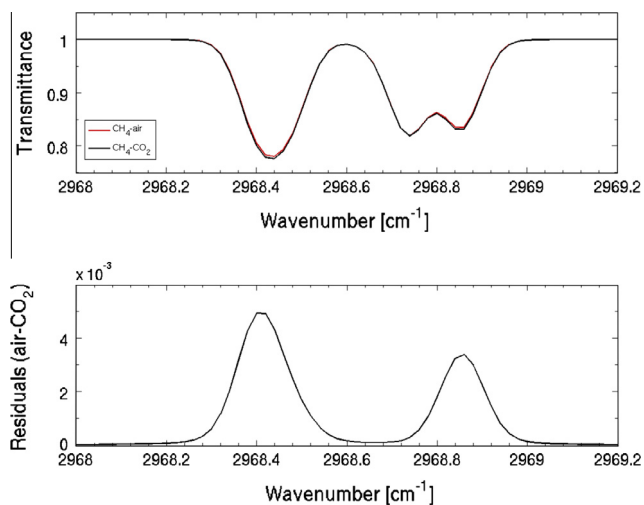


Fig. 7. ASIMUT simulations of the ν_3 band of CH_4 (30 ppb) in the solar occultation mode at a spectral resolution of 0.10 cm^{-1} using the conventional HITRAN parameters (air-broadened, red curve) and the data obtained in this work (CO_2 -broadened, black curve). Zoom on the P(5). The plots at the bottom represent the difference between the red and the black curve. (For interpretation of the references to color in this figure legend, the reader is referred to the web version of this article.)

low resolution of the NOMAD instrument, we consider the possible dependence as negligible and this approximation as reliable.

Spectra through the Martian atmosphere have been simulated with ASIMUT-ALVL, a LBL radiative transfer code [17]. It is a modular program for radiative transfer calculations in planetary atmospheres. Initially developed for the Earth atmosphere, its applicability has been extended to extraterrestrial atmospheres, such as those of Mars and Venus. The ASIMUT-ALVL software has been developed to exploit the synergy existing between the growing number of different instruments working under different geometries.

Input conditions were based on a southern summer Martian atmosphere model from the GM3 Mars GCM [31]. We used a

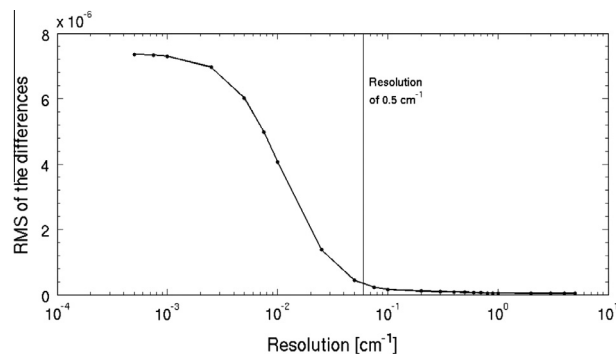


Fig. 8. Root mean square value of the difference (air - CO_2 broadening) in function of the spectral resolution used for the simulation of the nadir viewing mode. The X scale is logarithmic.

constant concentration of methane, of 30 ppb. ASIMUT-ALVL includes also the instrument function.

The resolution of NOMAD is planned to be between 0.10 and 0.30 cm^{-1} in solar occultation and in nadir viewing geometry, respectively. However spectra were simulated using Voigt profiles at various spectral resolutions, from 5 cm^{-1} down to $5 \times 10^{-4} \text{ cm}^{-1}$ to test the pertinence of using CO_2 broadened parameters and to infer the resolution at which the broadening effects might be of importance. Figs. 5 and 6 show simulations of the ν_3 band in nadir and in solar occultation viewing geometry respectively, using CO_2 broadening coefficients (black curve) and air broadening ones (red curve), at the NOMAD instrumental resolution. The plot in Fig. 7 presents a zoom-in on the P(5) lines simulated in Solar Occultation at a resolution of 0.10 cm^{-1} . The bottom panel shows the difference between the calculations obtained using HITRAN and the present values. The differences shown in Figs. 5–7 may seem quite small but at NOMAD's resolution they will matter. Using inaccurate lineshapes will increase uncertainties when fitting the experimental spectra. This may influence the results of the retrievals.

The differences obtained at each resolution were plotted in function of the spectral resolution. The results is shown in Fig. 8 for the nadir geometry. The evolution of the rms in function of the resolution presents an exponential profile for both geometries. It emerges that the use of one set of parameters plays a role starting at a resolution of 0.5 cm^{-1} . The difference is already noticeable at the theoretical resolution of NOMAD, as well in nadir as in solar occultation viewing modes.

6. Conclusion

In this paper, the CO_2 -broadening coefficients of 28 lines of CH_4 have been measured in the ν_4 band at room temperature using a tunable diode-laser spectrometer. The collisional widths have been individually deduced from Voigt, Rautian and Galatry model fits of each experimental lineshape. The residuals obtained with Voigt fits have always a typical signature while the other models are in excellent agreement with the experimental lineshapes. The values obtained were applied to 162 lines in the ν_3 band. We simulated Mars spectra in the Nadir and Solar Occultation observation modes at several resolutions.

Details on the composition and even the dynamics of a planetary atmosphere can be obtained by spectroscopy. Different instruments on board different satellites sound these atmospheres in different wavelength ranges, from the UV to the IR, under various geometries. Precise spectroscopic data to describe CO_2 pressure-broadened lineshapes of trace gases in the CO_2 rich atmospheres are rather scarce. Still the improvement of spectroscopic databases

sued for CO₂-rich planetary atmospheres [32,33] as well as up-graded space instruments [34] are necessary for a better characterization and understanding of our neighboring planets, Mars and Venus. Already at a resolution of 0.5 cm⁻¹, the set of CO₂-broadening parameters is of high importance to analyze spectra. As this resolution is technically achievable for flying instruments, we insist that accurate spectroscopic data will soon become essential in order to further characterize all kind of planetary atmospheres.

Acknowledgments

The research program was supported by the Belgian Federal Science Policy Office and the European Space Agency (ESA PRODEX program contracts C 90323, 90113, 17645, and C4000107727). Financial support from the Fonds de la Recherche Scientifique (F.R.S.-FNRS, contract FRFC) and the Action de Recherches Concertées of the Communauté française de Belgique is gratefully acknowledged. The research was performed as part of the Interuniversity Attraction Poles programme financed by the Belgian government (Planet TOPERS). We would like also to thank and acknowledge the support from the HiResMIR International Scientific Coordination Network (GDRI).

References

- [1] J.-M. Flaud, H. Oelhaf, C.R. Phys. 5 (2004) 259–271.
- [2] D.V. Titov, H. Svedhem, D. Koschny, R. Hoofs, S. Barabash, J.-L. Bertaux, P. Drossart, V. Formisano, B. Husler, O. Korabiev, W.J. Markiewicz, D. Nevejans, M. Ptzold, G. Piccioni, T.L. Zhang, D. Merritt, O. Witasse, J. Zender, A. Accommazzo, M. Sweeney, D. Trillard, M. Janvier, A. Clochet, Planet. Space Sci. 54 (2006) 1279–1297.
- [3] D. Nevejans, E. Neefs, E. Van Ransbeeck, S. Berkenbosch, R. Clairquin, L. De Vos, W. Moelans, S. Glorieux, A. Baeke, O. Korabiev, I. Vinogradov, Y. Kalinnikov, B. Bach, J.-P. Dubois, E. Villard, Appl. Opt. 45 (2006) 5191–5206.
- [4] J.-L. Bertaux, A.C. Vandaele, V. Wilquet, F. Montmessin, R. Dahoo, E. Villard, O. Korabiev, A. Fedorova, Icarus 195 (2008) 28–33.
- [5] G.L. Villanueva, M.J. Mumma, R.E. Novak, T. Hewagama, Icarus 195 (2008) 34–44.
- [6] V. Formisano, S. Atreya, T. Encrenaz, N. Ignatiev, M. Giuranna, Science 306 (2004) 1758–1761.
- [7] M.J. Mumma, G.L. Villanueva, R.E. Novak, T. Hewagama, B.P. Bonev, A.M. Mandell, M.D. Smith, Science 323 (2009) 1041–1045.
- [8] F. Lefèvre, F. Forget, Nature 460 (2009) 720–723.
- [9] R.W. Zurek, A. Chicarro, M.A. Allen, J.-L. Bertaux, R.T. Clancy, F. Daerden, V. Formisano, J.B. Garvin, G. Neukum, M.D. Smith, Planet. Space Sci. 59 (2011) 284–291.
- [10] S.K. Atreya, P.R. Mahaffy, A.-S. Wong, Planet. Space Sci. 55 (2007) 358–369.
- [11] A.C. Vandaele, F. Daerden, R. Drummond, E. Neefs, J.-J. López-Moreno, J. Rodriguez Gomez, M.R. Patel, G. Bellucci, the NOMAD team, NOMAD, a spectrometer suite for nadir and solar occultation observations on the ExoMars trace gas orbiter, in: 4th International Workshop on the Mars Atmosphere: Modelling and Observations, 2011.
- [12] R. Drummond, A.C. Vandaele, F. Daerden, D. Fussen, A. Mahieux, L. Neary, E. Neefs, S. Robert, Y. Willame, V. Wilquet, Planet. Space Sci. 59 (2011) 292–298.
- [13] M.A.H. Smith, C.P. Rinsland, V. Malathy Devi, D. Chris Benner, Spectrochim. Acta A 48 (1992) 1257–1272.
- [14] A.S. Pine, J. Quant. Spectrosc. Radiat. Transfer 57 (1997) 157–176.
- [15] M. Lepère, J. Mol. Spectrosc. 238 (2006) 193–199.
- [16] B. Martin, M. Lepère, J. Mol. Spectrosc. 259 (2010) 46–55.
- [17] A.C. Vandaele, M. DeMazière, R. Drummond, A. Mahieux, E. Neefs, V. Wilquet, D. Belyaev, A. Fedorova, O. Korabiev, F. Montmessin, J.-L. Bertaux, J. Geophys. Res. 113 (2008) E00B23.
- [18] M. Lepère, G. Blanquet, J. Walrand, J.-P. Bouanich, J. Mol. Spectrosc. 180 (1996) 218–226.
- [19] L. Fissiaux, G. Blanquet, M. Lepère, J. Quant. Spectrosc. Radiat. Transfer 113 (2012) 1233–1239.
- [20] A.G. Robiette, J. Mol. Spectrosc. 86 (1981) 143–158.
- [21] B.H. Armstrong, J. Quant. Spectrosc. Radiat. Transfer 7 (1967) 61–88.
- [22] P.L. Varghese, R.K. Hanson, Appl. Opt. 23 (1984) 2376–2385.
- [23] R.H. Dicke, Phys. Rev. 89 (1953) 472–473.
- [24] S.G. Rautian, I.I. Sobel'Man, Sov. Phys. Usp. 9 (1967) 701–716.
- [25] L. Galatry, Phys. Rev. 122 (1960) 1218–1223.
- [26] G. Blanquet, J. Walrand, J.-P. Bouanich, J. Mol. Spectrosc. 159 (1993) 137–143.
- [27] A. Mouchet, G. Blanquet, P. Herbin, J. Walrand, C.P. Courtoy, J.-P. Bouanich, Can. J. Phys. 63 (1993) 527–531.
- [28] M.A.H. Smith, D.C. Benner, A. Predoi-Cross, V.M. Devi, J. Quant. Spectrosc. Radiat. Transfer 111 (2010) 1152–1166.
- [29] L.S. Rothman, I.E. Gordon, A. Barbe, D.C. Benner, P.F. Bernath, M. Birk, V. Boudon, L.R. Brown, A. Campargue, J.-P. Champion, K. Chance, L.H. Coudert, V. Dana, V.M. Devi, S. Fally, J.-M. Flaud, R.R. Gamache, A. Goldman, D. Jacquemart, I. Kleiner, N. Lacome, W.J. Lafferty, J.-Y. Mandin, S.T. Massie, S.N. Mikhailenko, C.E. Miller, N. Moazzen-Ahmadi, O.V. Naumenko, A.V. Nikitin, J. Orphal, V.I. Perevalov, A. Perrin, A. Predoi-Cross, C.P. Rinsland, M. Rotger, M. Šimečková, M.A.H. Smith, K. Sung, S.A. Tashkun, J. Tennyson, R.A. Toth, A.C. Vandaele, J. Vander Auwera, J. Quant. Spectrosc. Radiat. Transfer 110 (2009) 533–572.
- [30] L.R. Brown, D.C. Benner, J.P. Champion, V.M. Devi, L. Fejard, R.R. Gamache, T. Gabard, J.C. Hilico, B. Lavorel, M. Loete, G.Ch. Mellau, A. Nikitin, A.S. Pine, A. Predoi-Cross, C.P. Rinsland, O. Robert, R.L. Sams, M.A.H. Smith, S.A. Tashkun, V.I. Tyuterev, J. Quant. Spectrosc. Radiat. Transfer 82 (2003) 219–238.
- [31] Y. Moudden, J.C. McConnell, J. Geophys. Res. 110 (2005) E04001.
- [32] M. Tudorie, T. Foldes, A.C. Vandaele, J. Vander Auwera, J. Quant. Spectrosc. Radiat. Transfer 113 (2012) 1092–1101.
- [33] R.R. Gamache, A.L. Laraia, J. Lamouroux, Icarus 213 (2011) 720–730.
- [34] V.J. Hipkin, P.O. Wennberg, G.C. Toon, J.R. Drummond for the MATMOS team, The Mars atmospheric trace molecule occultation spectrometer (MATMOS) on the 2016 EMTGO mission, in: EPSC Abstracts, EPSC-DPS2011-1746, vol. 6, 2011.